JOURNAL OF MATERIALS SCIENCE 29 (1994) 1833–1846

Surface reactivity of liquid metal with oxygen and its relationship with surface tension measurements: a kinetic–fluodynamic model

E. RICCI, A. PASSERONE, P. CASTELLO
Istituto di Chimica Fisica Applicata dei Materiali del C.N.R., Area della Ricerca del C.N.R., Via De Marini 6, I-16149 Genova, Italy

P. COSTA
Istituto di Scienza e Tecnologie Chimiche, Facoltà di Ingegneria dell'Università di Genova–Via all' Opera Pia, I-16145 Genova, Italy

A kinetic and fluodynamic description of processes that may take place near the liquid–vapour interface in the presence of an inert carrier flow containing definite oxygen amounts is presented, in relation to surface tension measurements. The evaluation of the Thiele modulus, ϕ, and of the parameter ε^0 (which compares the magnitude of the fluxes of interest to and from the surface), allows definition of the regimes in which fast or slow reactions in the gas phase surrounding a drop of liquid metal are possible in the presence of variable oxygen concentrations. The kinetic features of the process are described in terms of these different reaction regimes, and on the basis of the thermodynamic stability of the possible oxidation products. Diagrams on a plane $\log \phi^2/\log \varepsilon^0$ are drawn, immediately allowing one to know the range of $P^0_{O_2}$ and T in which the reaction considered is thermodynamically possible, and to foresee the evolution in this field from a kinetic point of view, as a function of $P^0_{O_2}$ and T. Therefore, the treatment presented here (and applied to selected cases of technological interest) allows a "stability field" for a chosen oxide on the $\log \phi^2/\log \varepsilon^0$ plane to be defined, and the behaviour of the system from a kinetic–fluodynamic point of view to be predicted when the flow parameters and the geometry of the experimental set-up are known. In particular, the reactive gas fluxes at the liquid–vapour interface can be evaluated as a function of the different experimental conditions. Kinetic–fluodynamic diagrams for liquid metal–oxygen systems containing Pb, Sn, Zn, Cu and Al are presented, as well as an application of the model to surface tension measurements on liquid tin, which gives semi-quantitative confirmation of the theory developed here.

1. Introduction

The reactivity of liquid metal surfaces with gases plays a significant role in several technological processes, such as brazing, soldering, alloying, crystal growth, formation of composite materials, etc. In all these cases, reactions occurring between a liquid metal and the working atmosphere can affect to a great extent the final results of a process.

It is well known that surface properties are strongly affected by the degree of cleanliness of a surface, which is dependent on the surrounding atmosphere, and in particular on its oxygen content. This gas is extremely surface-active for a large number of metallic systems [1]; its presence as a component of the biosphere, can never be completely avoided.

In order to relate the observed effects on surface properties to oxygen content in the experimental environment, the first critical point is to evaluate the effective gas concentration in the immediate surroundings of the surface, by understanding the physical and chemical processes that may take place in this layer.

The existence of an oxygen flux determining the adsorption process can be supposed; on the other hand, vaporization phenomena provide the existence of a flux of metallic vapours in the opposite direction. If the boundary conditions are favourable from both a thermodynamic and a kinetic point of view, it is possible that reactions will exist between the two elements in the gas phase, in the vicinity of the surface. This will cause both an increase in the metal vaporization rate and a decrease in the oxygen content of the gaseous layers in contact with the liquid surface; the contamination of the surface itself could consequently be reduced.

The effect of oxygen partial pressure on the vaporization rate of metals has been studied by Turkdogan *et al.* [2]. They observed that enhancement of the vaporization rate of metals must be expected, and depends linearly on the oxygen content of the surrounding gaseous atmosphere. On the other hand, it has been pointed out [3, 4] that some anomalous trends in surface tension versus temperature, can be

0022–2461

justified by considering different availabilities of oxygen near the surface as a function of temperature and gas flow rate.

A dynamic description of the processes that may take place near the surface of liquid metals in the presence of definite oxygen partial pressures has been given previously [5]. The aim of this paper is to widen the theoretical model developed in [5] and to apply it to a certain number of metals, with particular emphasis on their thermodynamic properties; providing for each a model of behaviour in different thermodynamic and fluodynamic conditions, with reference to typical experimental conditions used in surface tension investigations.

2. The model and its description in terms of reaction regimes

High temperature measurements of surface tension are commonly performed by sessile or levitating drop methods [6]. The experimental apparatus for both these techniques consists of a tube-shaped vacuum tight chamber in which a drop of pure element or alloy is placed, and where a gaseous flux of known composition is introduced.

Oxygen concentration in the gas flow can be controlled in two different ways:

1. by mixing known amounts of this gas with an inert carrier, like helium or argon; and
2. by using gaseous mixtures, like CO/CO_2 or H_2/H_2O, able to provide oxygen as a product of chemical equilibrium.

In such mixtures, the oxygen concentration is defined at each temperature by the initial concentration of the other species and by the equilibrium constant of the reaction.

High vacuum conditions are also very often used but they will not be treated here. For the sake of clarity the assumptions of the model, extensively described in the previous work [5], are briefly reported here.

1. Atmosphere: helium (carrier gas) + O_2 at defined partial pressure $P^0_{O_2}$, with a total pressure, P_{tot}, of the order of 0.1 MPa (where 0 is a quantity referred to the gas supply).
2. The liquid surface is "plane", i.e., the drop diameter, d_d, is "large" as far as capillary effects are concerned. The exchange surface of the drop is indicated as S_d.
3. The initial oxygen content of the liquid metal is equal to zero.
4. The temperature is uniform in a large region of the tube-shaped chamber (having a section S_t), surrounding the drop.
5. Gas flow can be considered as laminar. The flow condition can be checked through an evaluation of the Reynolds number of the drop (laminar flow for $Re < 100$).
6. Only the formation of the most stable oxide in the imposed conditions of $P^0_{O_2}$ and temperature, (T) is considered, via the reaction:

$$M^{gas} + \alpha O_2^{gas} \rightarrow MO_{2\alpha}^{condensate} \quad (1)$$

where M is the molecular weight of the metal (g) and α is the stoichiometric coefficient.

7. The vapour pressure of the oxide is considered negligible. This allows one to ignore the presence of the oxide in the vapour phase.
8. The theory developed until now is based on the so called "effective film theory" [7]. At a distance, δ_t, from the drop, the oxygen partial pressure is assumed to be constant and corresponds to a certain value $P^p_{O_2}$, where p indicates a quantity referred to the atmosphere at the diffusion boundary layer. This can be estimated from a material balance involving the oxygen supply at $P^0_{O_2}$, the oxygen outlet and the oxygen flux towards the drop.

The thickness of the diffusion layer, δ_t, and $P^p_{O_2}$ values, together with the assumption of initial zero oxygen content of the metal surface, define a diffusion profile around the drop. Depending on the flow parameters and on the geometry of the experimental set-up, three such types of diffusion profile can be singled out, as shown in Appendix 1.

9. Molecular diffusion is assumed to be the process mainly controlling the exchange of matter between the drop and the surrounding atmosphere. Obviously, the diffusivity coefficient D for the layer becomes meaningless when the mean free path is greater than the thickness. Thus, high vacuum conditions are explicitly ruled out of consideration in the present treatment. A schematic layout of the model is presented in Fig. 1.

2.1. ϕ parameter

The Thiele modulus [8, 9], ϕ is a dimensionless quantity referring to a process in which reactants reach, via diffusion, the site where the reaction itself takes place. The square of this quantity defines the ratio between the reaction and the diffusion rates; this value can be more or less than one, and the slow stage of the whole process corresponds, respectively, to the reaction or to the diffusion regimes.

In the case of the model, assuming that Equation 1 is of first order for each reactant, the expression for ϕ^2 becomes:

$$\phi^2 = \frac{\delta_t^2 \alpha P^s_{met} k}{D_{O_2} P_{tot}} \quad (2)$$

Where P^s_{met} is the vapour pressure (s signifying on equilibrium constant) of the liquid metal, D_i is the diffusion coefficient of the species "i" in helium and k is

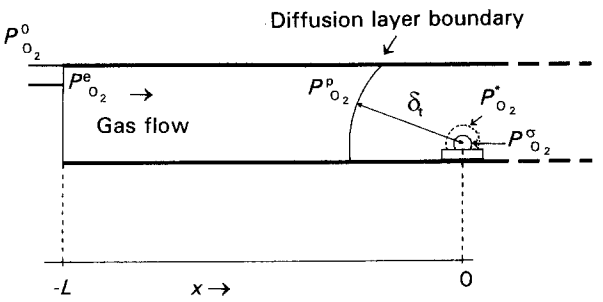

Figure 1 Schematic layout of the experimental set-up for surface tension measurements.

the kinetic constant of the reaction. This constant is not known, as far as we know, for most of the reactions occurring between metal vapours and oxygen at high temperatures. Thus, it can be calculated, as a first approximation, as the total number of collisions between metallic atoms and oxygen molecules in the gas phase, disregarding the existence of an activation threshold. In spite of this approximation, which finally leads to an over-estimation of the Thiele modulus, the values of k obtained by calculation are in reasonable agreement with the few experimental data one can find in literature [5].

2.2. ε^0 parameter

ε^0 is a dimensionless quantity defined as:

$$\varepsilon^0 = \frac{\alpha D_{met} P^s_{met}}{D_{O_2} P^0_{O_2}} \quad (3)$$

ε^0 compares the magnitudes of the flux of matter in two opposite directions. By calculating the quantities ϕ^2 and ε^0, respectively, by Equations 2 and 3 for a definite process and fixed boundary conditions, one can define the state of the system from a kinetic and diffusional point of view; and describe its behaviour in terms of the following four reaction regimes, depending on the relative value of the two parameters [10, 11].

1. Regime A: the reaction is slow with respect to diffusion (for $\phi^2 \ll 1, \phi^2 \ll \varepsilon$). The chemical reaction is the slow stage of the process. Oxygen diffusion and metal vaporization are not influenced by the oxidation process, and oxygen has time enough to reach the metallic surface and to diffuse into the drop before reacting.

2. Regime B: fast reactions with oxygen excess (for $\varepsilon \ll \phi^2 \ll 1/\varepsilon$). The diffusion of metal vapours is the slow stage of the process, and oxidation is confined at the liquid surface. Reaction causes only enhancement of the metal vapour flux.

3. Regime C: fast reactions with metal vapour excess (for $1 \ll \phi^2 \ll \varepsilon^2$). This is the opposite case; the slow stage is the oxygen diffusion, and oxidation is confined in proximity to the upper limit of the effective film. Reactions determine only the enhancement of the oxygen flux.

4. Regime D: instantaneous reactions (for $\phi^2 \gg (1/\varepsilon)$, $\phi^2 \gg \varepsilon^2$). The chemical reaction is the fast stage of the process, while diffusion of both gaseous species is slow. Both fluxes are enhanced by oxidation, which is confined by the balance of diffusional fluxes into a definite thin layer of the effective film, the reaction plane ($\Sigma_{reaction}$), whose distance from the metallic surface is given by:

$$\Sigma_{reaction} = \varepsilon\delta_t/(1 + \varepsilon) \quad (4)$$

with $\varepsilon = \varepsilon^0(P^0_{O_2}/P^p_{O_2})$.

The borderlines of the different regions are defined, in the most general form, by the following equations:

Regime A–regime B:

$$\log\varepsilon^0 = \log\phi^2 + \log(P^p_{O_2}/P^0_{O_2}) \quad (5)$$

Regime D–regime B:

$$\log\varepsilon^0 = (-\log\phi^2) + \log(P^p_{O_2}/P^0_{O_2}) \quad (6)$$

Regime A–regime C:

$$\log\phi^2 = 0 \quad (7)$$

Regime C–regime D:

$$\log\varepsilon^0 = \log\phi^2 + \log[(P^p_{O_2})^2/(P^0_{O_2})^2] \quad (8)$$

As the transition from one region to another is not sharp, the borderlines defined by Equations 5 to 8 have been spread into bands. Each band represents a transition region between two reaction regimes, and is approximately one order of magnitude wide.

Equations 5 to 8 show that the position of the rigorously calculated borderlines (i.e. the relative extension of the regions associated with the different regimes) changes under different thermodynamic and fluodynamic conditions, even if not to a large extent.

Considering the stoichiometry of the formation reaction of a metal oxide, the thermodynamic conditions (atmosphere composition and T) and the fluodynamic features of the system (flow rate, geometry of experimental apparatus), a couple of ϕ^2 and ε^0 values can be calculated for a given metal–oxygen system under definite boundary conditions. This couple identifies one point on the plane $\log\phi^2/\log\varepsilon^0$. Its position can be used to define the kinetic–diffusional state of the system itself in terms of the corresponding reaction regime.

2.3. Delimitation of the regions associated with the different regimes

Special care has to be taken when drawing the diagram and placing the representative points of a system, in order to be sure that the points and the borderlines have been evaluated with respect to the same boundary conditions.

For instance, at low flow rates, having defined a shape factor, $f = S_t/S_d = d_t^2/d_d^2$, the condition $f\,Pe_{film} \leq Pe_t \ll 1$, is verified (see Appendix 1); where d_t is tube diameter and Pe is the Peclet number. The diagram assumes the shape in Fig. 2. On the contrary, at high flow rates ($f\,Pe_{film} \gg 1$), the borderline C–D shall lie on the X-axis.

When substituting the appropriate expression of P^p_A (Appendix 1) in Equations 5 to 8, the slope of each line depends on the gas flow parameters (linear dependence) and on the temperature (dependence 3/2). Since this dependence is smoothed out by the logarithm, the slope of the borderlines can be considered, as a first approximation, to be constant with T, and can be calculated for an average value of the quantity D_{O_2}. Variation of this parameter in the range of one order of magnitude can produce displacements of the borderlines not greater than one logarithmic unit.

Much more attention is required when the flow rate or the geometry of the experimental set-up are changed; in these cases it is necessary to verify the correct position of the borders, which depend on relative values of Pe_t and $f\,Pe_{film}$, according to the criteria presented in Appendix 1.

As a final consideration, it is pointed out that in the definition of the Thiele modulus for the model described in this paper, an order of reaction equal to two has been assumed; first order for each reactant. This assumption is supported by the few experimental data that are available. However, the diagram itself could be used as an instrument to investigate the kinetics through an iterative process.

Assuming that one is able to determine the boundary conditions, both thermodynamic and fluodynamic, for which a given metal–oxygen system encounters a transition between two of the four described reaction regimes, one could substitute Equation (3) with another expression for ϕ^2 that gives a better account of the experimental data. In the same way, investigations on the rate constant of reaction k could be made, finding its "best value" through sequential approximations.

3. Characteristic diagrams for a given metal–oxygen system

For definite fluodynamic conditions a characteristic zone in the plane log ϕ^2/log ε^0 exists where any point related to a certain oxidation process occurring in a given metal–oxygen system can be placed: the position and the width of this zone are defined by the thermodynamic properties of the system, and in particular by the chemical stability of the species taking part in the process considered.

It must be remembered that ϕ^2 and ε^0 are calculated with reference to a well defined reaction, with its own stoichiometry. The only values of these two parameters that must be taken into consideration are those corresponding to coupled values of $P^0_{O_2}$ and temperature, for which the chemical stability of the compound indicated as the product of that reaction is greater than the analogous quantity for:
(a) reactants; and (b) possible products of any other process. These coupled values, lead to define a stability field in Fig. 2; this zone represents the kinetic–fluodynamic diagram of a given system for a selected reaction, all the points which fall out of this zone no longer have any physical significance.

All the information contained in a stability diagram T/P_{O_2} [12, 13] can be suitably translated on the plane log ϕ^2/log ε^0. The results of such a procedure are presented in the following, with reference to metals for which assessed data on the stability of both the pure metal and its different oxides can be found [14].

A detailed example of the calculation of a log ϕ^2/log ε^0 diagram is given for the lead–oxygen system, for which the reaction:

$$Pb^{gas} + \tfrac{1}{2} O_2^{gas} \rightarrow PbO^{condensate} \quad (9)$$

has been considered.

3.1. Temperature

One of the assumptions of the model is the presence of the metal in its liquid form; thus, only co-ordinate points, log ϕ^2, log ε^0, corresponding to T values for which the liquid form of the metal exists must be taken in consideration.

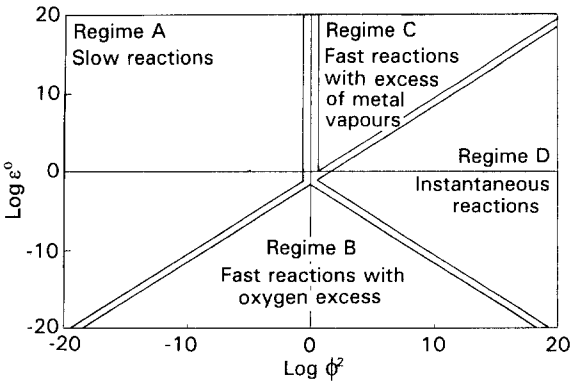

Figure 2 General form of the kinetic–fluodynamic diagram for low laminar flows.

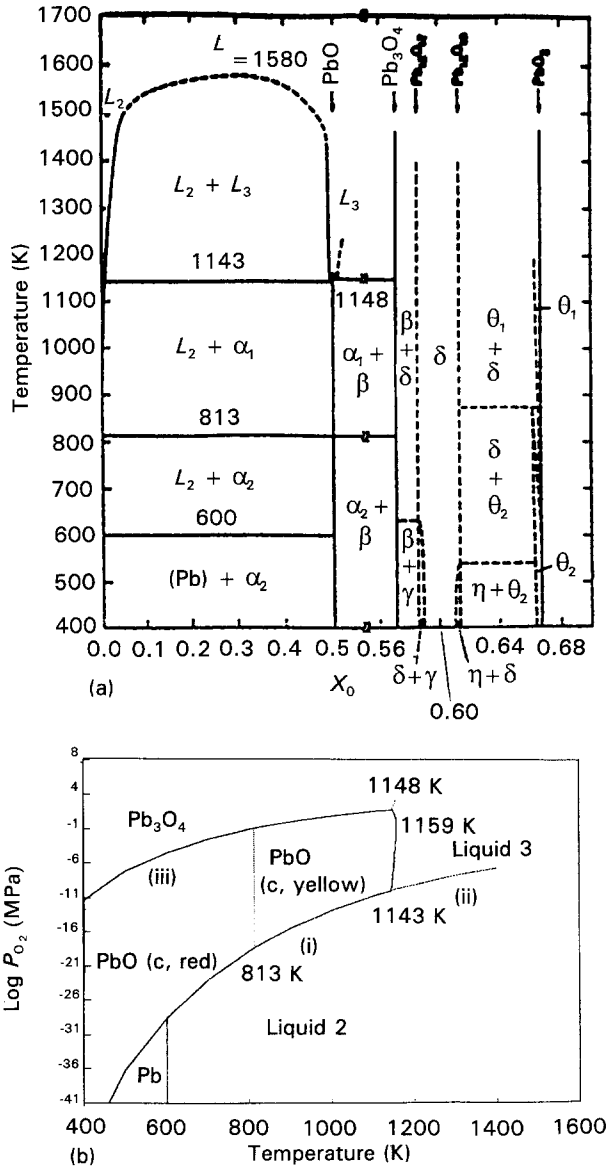

Figure 3 (a) Phase diagram of the system Pb–O [12], and (b) stability diagram of the system Pb–O (from data in [14]).

The lower temperature limit of the diagram is then the melting point of pure lead, (601 K). As an upper limit a temperature of 1500 K can be assumed, being that the behaviour of liquid PbO is unknown for temperatures higher than 1500 K, resulting from Fig. 3a. Above this temperature, as can be seen in Fig. 3b, Pb_3O_4 can be formed, under oxygen pressures $> 1.013 \times 10^5$ Pa.

The characteristic zone for Equation 9 is consequently comprised between two straight lines, whose points must have co-ordinates, log ϕ^2 and log ε^0, calculated for T equal to each one of these two temperatures. From the definition of ϕ^2 and ε^0, it follows that these isothermal lines must be vertical ones, i.e. lines at constant ϕ^2.

3.2. Equilibrium values of oxygen partial pressure in the oxidation reactions

As can be seen in Fig. 3b, PbO formation is thermodynamically favoured only in the field delimited by the lines marked with symbols (i), (ii) and (iii), corresponding, respectively, to the equilibria between the following phases:

(i) $L_2 - PbO^{crystal}$,
(ii) $L_2 - L_3$, and
(iii) $Pb_3O_4^{crystal} - PbO^{crystal}$.

Three series of $P^0_{O_2}$ and T values corresponding to each one of these equilibria, define the borderlines of the stability field of PbO on the stability diagram. By Equations 3 and 4, three series of ϕ^2 and ε^0 values, corresponding to those values, can be calculated, in order to obtain three other lines delimiting the characteristic zone of Equation 1 on the plane log ϕ^2/log ε^0.

As a first approximation we can suppose the equilibrium (i), L_2-PbO crystal, to correspond to the reaction

$$Pb^{liquid} + \tfrac{1}{2}\,O_2^{gas}\ PbO^{crystal} \qquad (10)$$

The equilibrium values of $P^0_{O_2}$ can be calculated at each temperature from thermodynamic data [14], and corresponding limiting values of ϕ^2 and ε^0 can be obtained by Equations 2 and 3. These couples (ϕ^2, ε^0) locate the points on the straight line (i) in Fig. 4, i.e. the analogous of line (i) in Fig. 3b.

Points defining (ii) line can be determined in the same way with reference to the reaction:

$$Pb^{liquid} + \tfrac{1}{2}\,O_2^{gas} \rightarrow PbO^{liquid} \qquad (11)$$

Finally, points defining the (iii) line can be determined with reference to the reaction:

$$3PbO^{crystal} + \tfrac{3}{2}\,O_2^{gas}\ Pb_3O_4^{crystal} \qquad (12)$$

Kinetic–fluodynamic diagrams for systems containing Sn, Zn, Al and Cu, are also presented in Figs 5 to 8; they have all been constructed in the same way as for the lead–oxygen system.

3.3. Total pressure

The significant zone of the log ϕ^2, log ε^0 plane is defined not only by the limiting values of $P^0_{O_2}$ and T, but also by the total pressure imposed: in fact, considering points of the diagram corresponding to oxygen pressures larger than the limit value fixed for the total pressure (for instance, 0.1 MPa) has no significance at all. Thus, another borderline of the characteristic zone is then drawn by joining all the points of the log ϕ^2, log ε^0 co-ordinates calculated for $P^0_{O_2} = 0.1$ MPa.

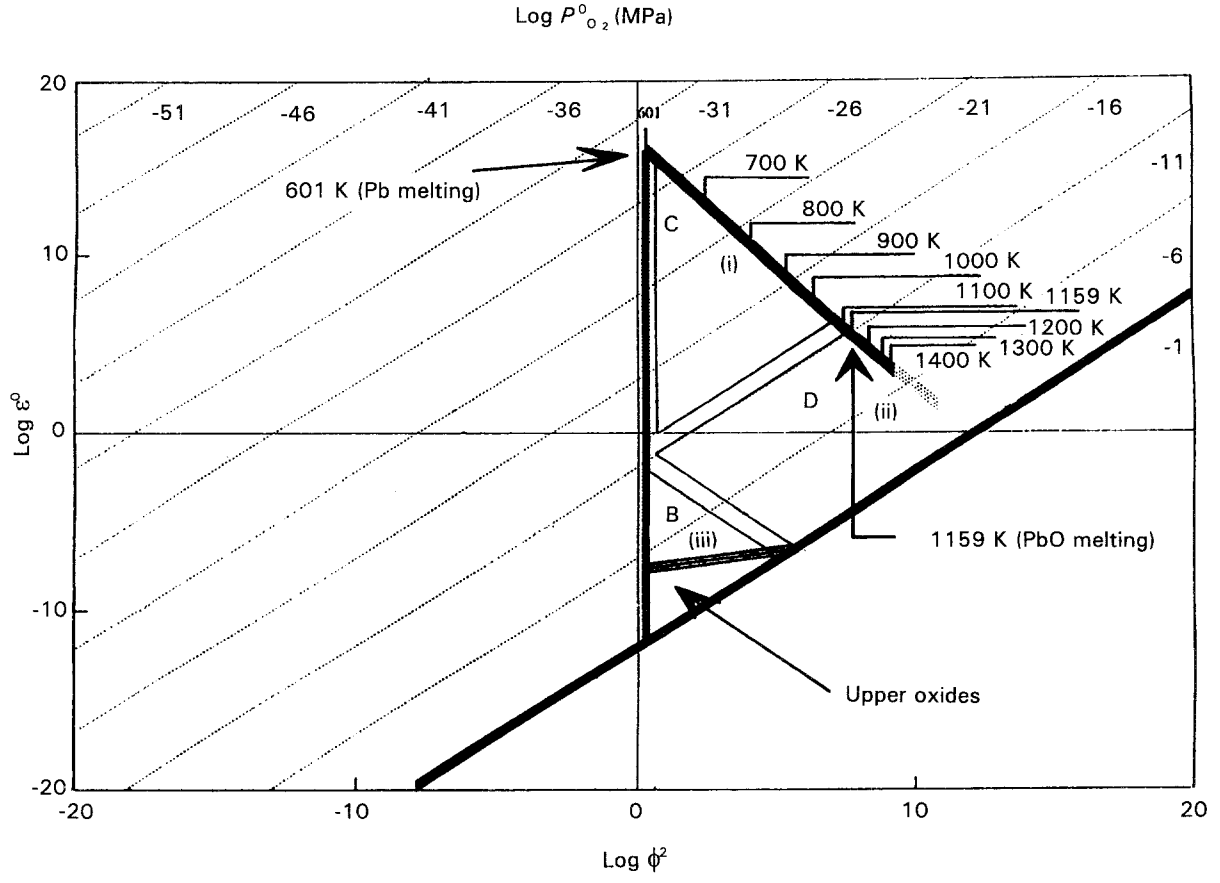

Figure 4 Kinetic–fluodynamic diagram for the lead–oxygen system; reaction $Pb^{gas} + \tfrac{1}{2}\,O_2^{gas} \rightarrow PbO^{condensate}$

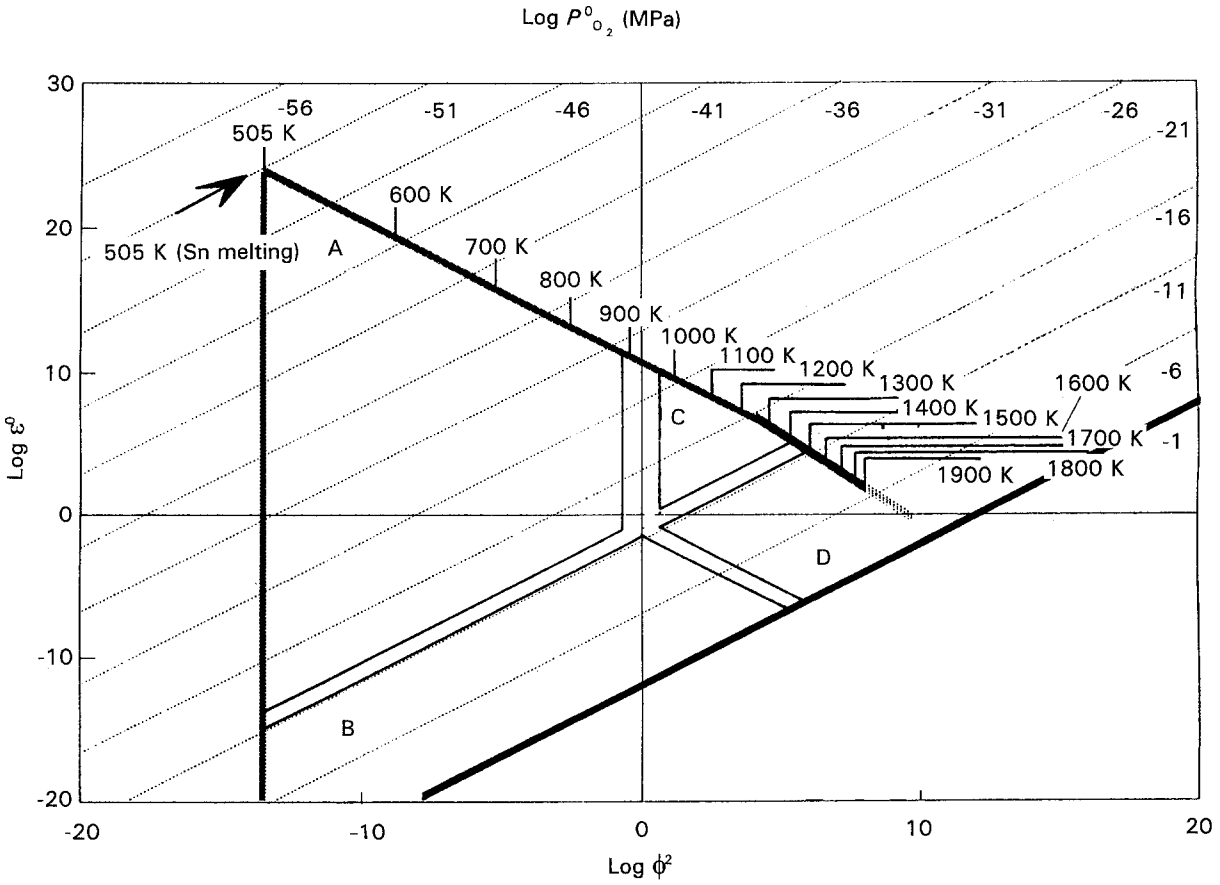

Figure 5 Kinetic–fluodynamic diagram for the tin–oxygen system; reaction $Sn^{gas} + O_2^{gas} \rightarrow SnO_2^{condensate}$.

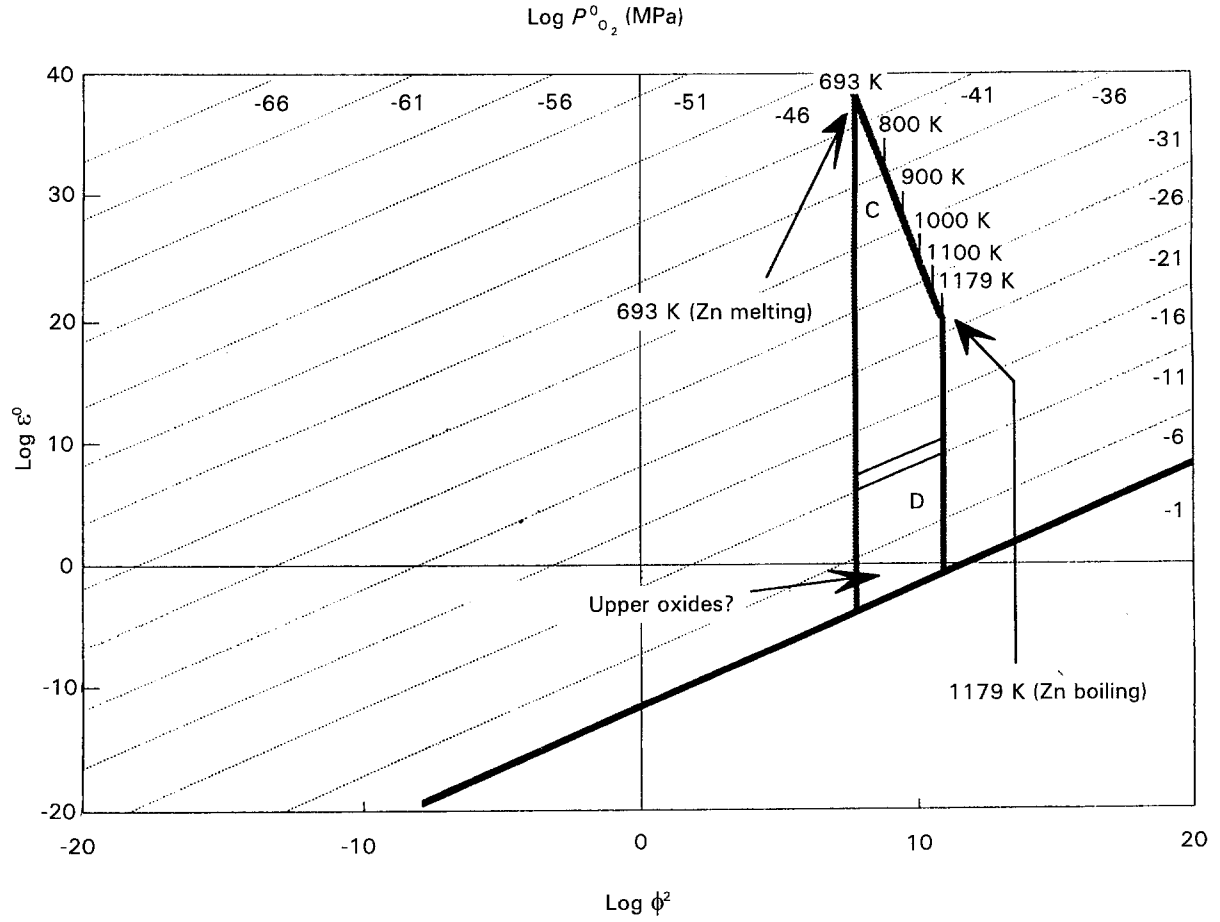

Figure 6 Kinetic–fluodynamic diagram for the zinc–oxygen system; reaction $Zn^{gas} + \frac{1}{2} O_2^{gas} \rightarrow ZnO^{condensate}$.

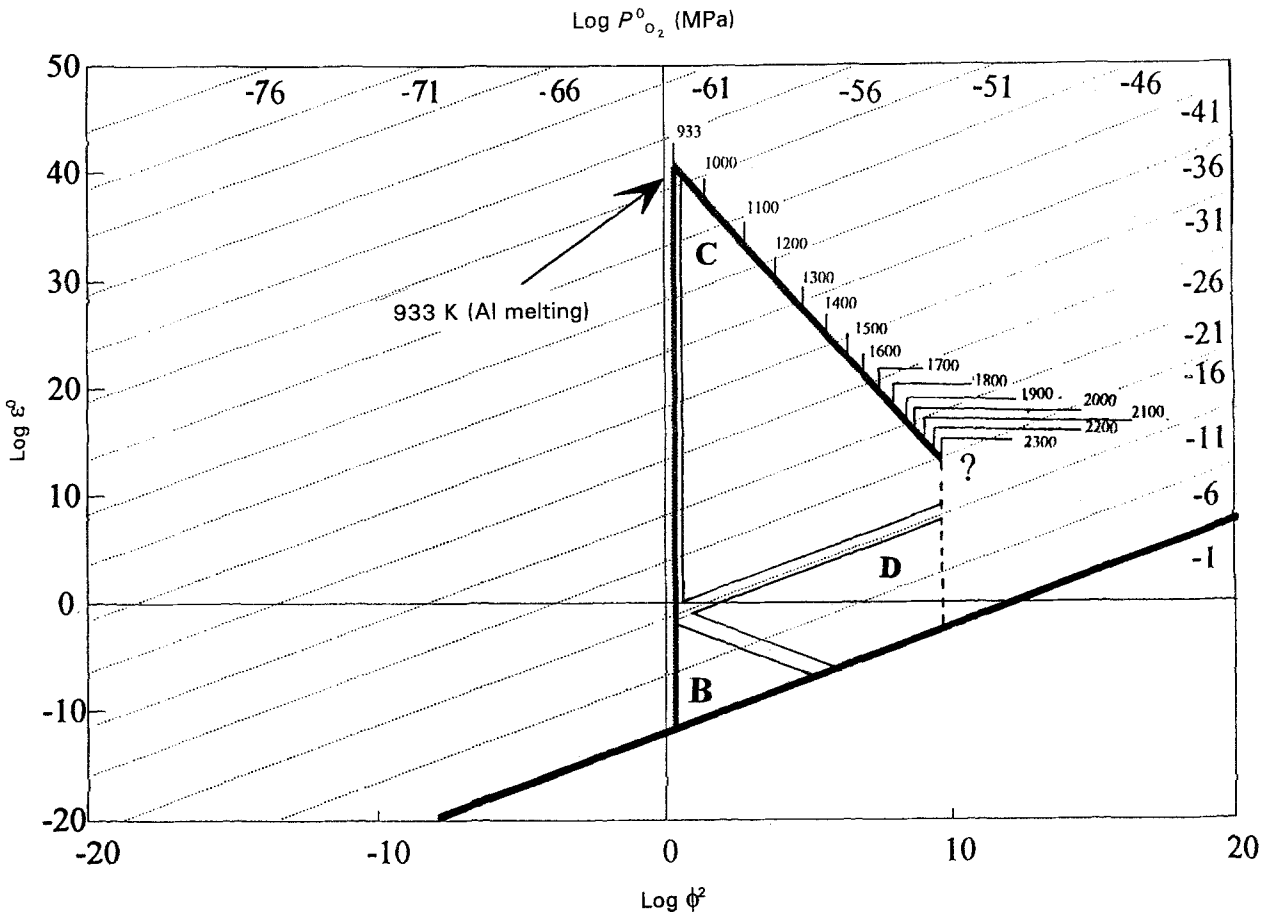

Figure 7 Kinetic–fluodynamic diagram for the aluminium–oxygen system; reaction $2Al^{gas} + \frac{3}{2} O_2^{gas} \rightarrow Al_2O_3^{condensate}$.

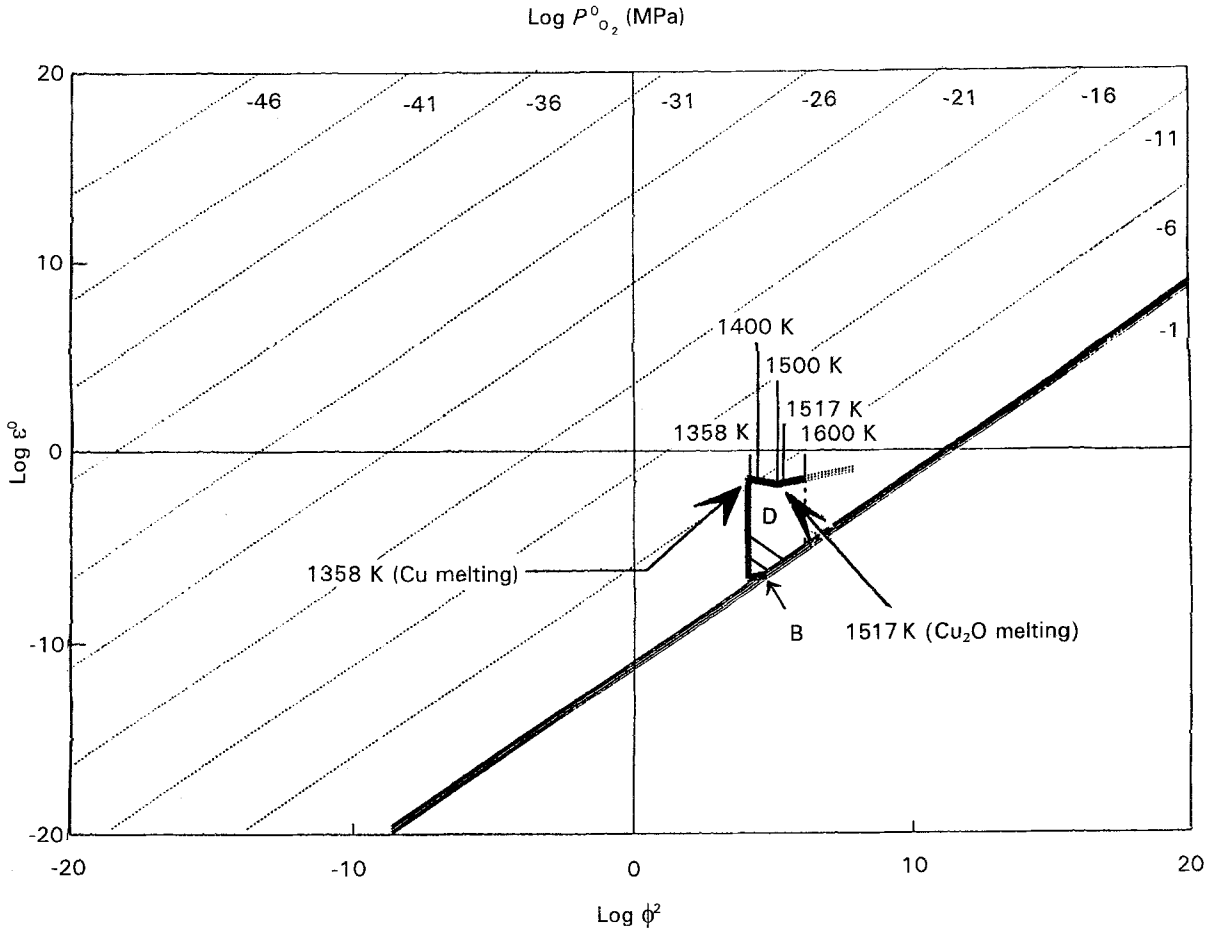

Figure 8 Kinetic–fluodynamic diagram for the copper–oxygen system; reaction $2Cu^{gas} + \frac{1}{2} O_2^{gas} \rightarrow Cu_2O^{condensate}$.

4. Visualization of thermodynamic parameters $P^0_{O_2}$ and T on the kinetic– fluodynamic diagram

From the definitions of ϕ^2 and ε^0 it can be seen that:

$$\log \varepsilon^0(T) = \log \phi^2(T) - \log\left[\frac{\delta_t^2 k(T) P^0_{O_2}}{P_{tot} D_{met}(T)}\right] \quad (13)$$

The second term on the right-hand side depends on the T through $k(T)$ (dependence 1/2) and $D_{met}(T)$ (dependence 3/2). However, the resulting linear dependence on T is smoothed out by the logarithm. For this reason, as a first approximation, the second term on the right can be considered nearly constant with T; thus, the values of log ε^0 calculated at different temperatures, but at one single value of $P^0_{O_2}$, are represented by a straight line having unitary slope.

It can be easily demonstrated that by varying the value of oxygen partial pressure a family of straight lines is obtained whose separation is linear with ΔP. Thus, isobaric lines can be drawn, allowing interpolation and extrapolation of data to be easily made with reference to the oxygen imposed partial pressure.

The dependence of ϕ^2 and ε^0 from T is less straightforward, deriving from quantities like diffusivity, vapour pressure and reaction kinetics; so, in order to draw a family of isothermal straight lines, log ϕ^2, must be evaluated for just one value of $P^0_{O_2}$, for each desired temperature. Then, isothermal vertical lines passing through these calculated points can be drawn.

5. Discussion

Several indications can be found in the literature to support the idea that metal vaporization plays a fundamental role in surface oxidation kinetics. An inversion of the slope of surface tension versus T when the temperature is lowered has been observed by White [15] and by Nogi *et al.* [3] on zinc; both these authors relate this effect to increased surface contamination. The decrease of metal vapour pressure with decreasing temperature enhances the accessibility of oxygen to the surface. This means increasing accessibility of oxygen to the surface being the gas flux, no longer "contrasted" by a counter flux of metal vapours.

Similar deviations from linearity can be found in data reported by Nizhenko *et al.* [16] and by Hardy [17] on the surface tension of liquid gallium.

Goumiri and Joud [18] made observations on the oxidation kinetics of aluminium surfaces by Auger electron spectroscopy (AES). They demonstrated that oxidation proceeds much more rapidly on solid than liquid aluminium, although the reaction is thermodynamically favoured in both cases. Solid Al is rapidly covered by a thin oxide layer under an oxygen partial pressure 10^{-18} MPa, while the liquid Al surface becomes cleaner under a pressure ten times greater.

Sangiorgi *et al.* [19], in studying surface tension of liquid tin–oxygen alloys in relation to surface composition investigated by AES, have observed that no oxidation of the tin liquid surface can be appreciated for 2 h under an oxygen pressure of 4×10^{-12} MPa, which is thermodynamically largely sufficient to promote the formation of the oxide.

Although the experimental set-up used in all these experiments was somewhat different from those assumed for our model, the common feature of the observations reported by the different investigators seems to support our theory.

5.1. Calculation of oxygen fluxes towards the metallic surface

In order to forecast the influence of oxygen on surface tension measurements of liquid metals, an evaluation of the oxygen fluxes towards the surface at the liquid–gas interface, $N^s_{O_2}$, has to be made. General equations allowing this kind of estimation are presented in Appendix 2 for each reaction regime.

When $N^s_{O_2}$ is known, it becomes possible to evaluate the time that the liquid metal needs to reach the equilibrium content of oxygen. The time needed for bulk saturation of the liquid drop, θ_b, is:

$$\theta_b = \frac{X^s_O \rho V_d}{M S_d N^s_{O_2}} \quad (14)$$

where ρ is the liquid metal density (g cm^{-3}), M is the molecular weight of the metal (g); V_d and S_d are, respectively, the drop volume and the exchange surface; and X^s_O is the bulk oxygen molar fraction at saturation. This last quantity corresponds to the limit of the solubility value of oxygen [20] when the reaction becomes thermodynamically possible ($P^0_{O_2} > P^s_{O_2}$) and, as a first approximation, to the value given by Sievert's law [1] when no reaction takes place ($P^0_{O_2} < P^s_{O_2}$).

Neglecting diffusion of the surface adsorbed oxygen into the liquid metal, a time can also be calculated to form an adsorbed oxygen monolayer:

$$\theta_m = \frac{\Omega}{N^s_{O_2}} \quad (15)$$

where Ω is the number of surface sites per unit area (mol cm^{-2}) [5] (typical values for $\Omega \approx 3 \times 10^{-9}$ mol cm^{-2}).

5.2. Application of the model to surface tension measurements on liquid tin

A semi-quantitative confirmation can be found in data collected by Passerone *et al.* [4] in a work on the influence of oxygen on the surface tension of liquid tin (Fig. 9). The straight line in Fig. 9 represents the trend of surface tension versus temperature, and connects experimental values obtained under boundary conditions that can be assimilated to those of the model, under an oxygen partial pressure of 10^{-21} MPa. These values are marked with squares.

All other points have been obtained under the same helium total pressure of 0.1 MPa but with higher partial pressures of oxygen, ranging from 10^{-7} to 10^{-11} MPa. As one would expect, in the presence of higher environmental oxygen concentrations, surface tension values are in general lower along the whole temperature range; but, in addition, a sharp decrease with respect to the linear trend obtained at $P^0_{O_2} = 10^{-21}$ MPa can be observed below 900 K.

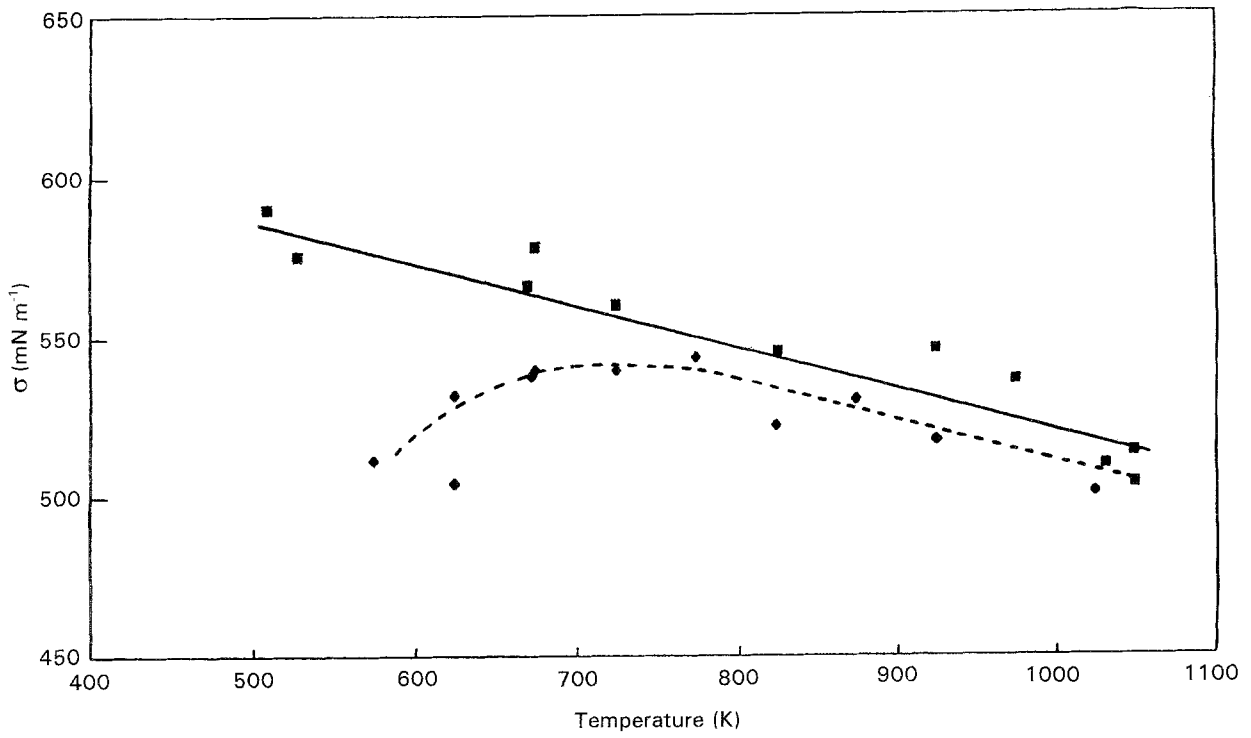

Figure 9 Surface tension of liquid tin measured under helium–oxygen atmospheres (after [4]). (■) $P_{O_2} = 10^{-21}$ MPa, (◆) $P_{O_2} = < 10^{-11}$ MPa.

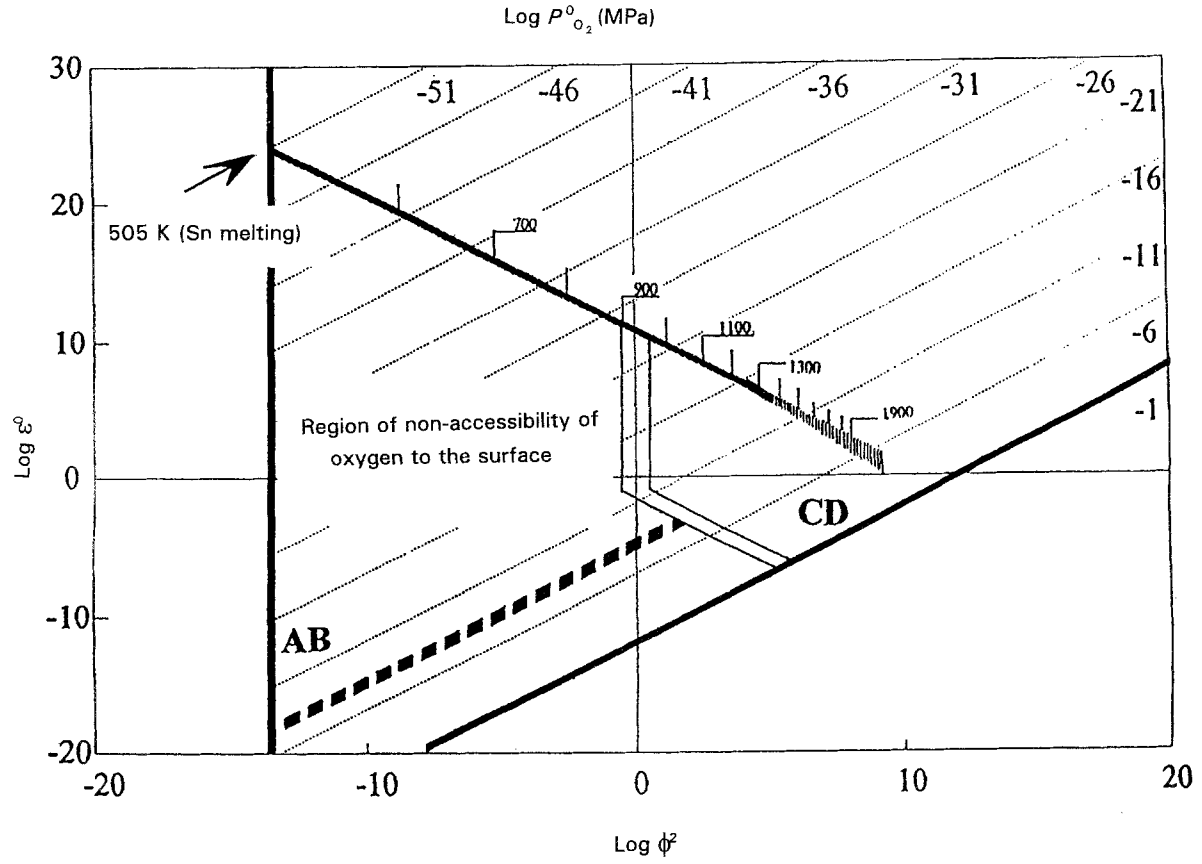

Figure 10 Simplified kinetic–fluodynamic diagram for the tin–oxygen system.

In order to relate these observations with the kinetic–diffusional theory here developed, the diagram for the system Sn–O (Fig. 5) can be simplified in the following way:

1. Neglecting the division between regions C–D and A–B, the log ϕ^2, log ε^0 plane can be considered as divided simply into two areas AB and CD; the first corresponds to the regimes in which oxygen reaches the surface, and the other to the ones in which this does not happen (Fig. 10).

2. Considering the duration time of measurements, and calculating the time oxygen needs to reach the

surface in definite thermodynamic and fluodynamic conditions by Equation 15, a zone in the AB region can be delimited in which the oxygen flux towards the surface is so low that contamination can be considered to be not taking place at all. This is because the oxygen does not have enough time to reach the surface during the experiment. The dashed line in Fig. 10 indicates these limiting thermodynamic conditions (calculations made in order to draw this line are shown in Appendix 3).

Points calculated for $P^0_{O_2} = 10^{-21}$ MPa lie in the region corresponding to the reaction regime CD for $T > 950$ K, and to the reaction regime AB for lower T. At high temperatures, the oxidation reaction of Sn should take place far from the liquid surface; which should therefore remain clean. When T is lowered, the system $Sn^{liquid} + O_2$ enters the zone of the region AB, in which the oxygen flux towards the metal [5] can be neglected. Selected values of $N^s_{O_2}$, θ_b and θ_m for the tin–oxygen systems from [4] are given in Table I.

According to the kinetic–fluodynamic model for Sn, lowering T from about 1000 K under $P^0_{O_2} = 10^{-21}$ MPa, the liquid surface should remain clean, and surface tension measurements should not suffer any interference from the oxide formation reaction. This is in good agreement with the experimental trend, as shown by the squares (Fig. 9).

When $P^0_{O_2}$ value is raised up to 10^{-11} MPa, points on the diagram calculated for $T > 950$ K again lie in the CD region, so the surface should be reasonably clean. When T is lowered, the system enters the AB region. Here again no reliable effects are observed, according to the evaluation of the oxygen fluxes towards the surface (Table I). For $P^0_{O_2} = 10^{-7}$ MPa and $T \sim 1000$ K, the system definitely enters the region in which the oxygen flux at the liquid metal–gas interface is really significant, and oxygen is expected to saturate the surface in a very short time.

According to Fig. 10, this decrease should take place at about 1000 K; whereas the experimental points start deviating from a straight line at about 800 K. This disagreement with the experimental data, even if not very important, can be accounted for by the following:

1. Experimental data are scattered, so that it is not easy to state, with a good level of accuracy, at which temperature the surface tension begins to fall.

2. The existence of a certain degree of approximation must be accounted for by the position and width of the borderline between regimes CD and AB. A transition between these two regimes with diminishing T, softer than the one presented in Fig. 10, is to be expected.

5.3. Application of the kinetic–fluodynamic model to more than one reaction

The diagrams presented in this paper refer to the formation reaction of one definite compound in a given metal–oxygen system. If the boundary conditions chosen are such as to render that reaction the most probable, this can be considered correct. Knowing data about the stability of all different possible oxides in different thermodynamic conditions, one can define the range of partial pressures of oxygen and temperature in which the formation of a certain oxide is favoured with respect to those of all others. On the basis of this information, the discussion about kinetic–fluodynamic aspects can be developed with reference to a certain reaction which is defined by the thermodynamic conditions.

In Fig. 4 a region where the formation of compounds richer in oxygen than PbO is expected, has been drawn. One of these compounds is Pb_3O_4. Knowing the thermodynamic conditions in which this oxide is stabler than all other, one could draw a diagram analogous to that in Fig. 4, referring to the reaction:

$$3Pb^{gas} + \tfrac{1}{2} O_2^{gas} \rightarrow Pb_3O_4^{crystal} \qquad (16)$$

Applying Equations 2 and 3 simply accounts for the different stoichiometry.

Nevertheless, this is not very interesting for studying the oxygen effects on surface tension; indeed, when a quantity of oxygen, corresponding to stoichiometry of the lower oxide, has been adsorbed on the surface, the surface tension tends asymptotically towards a minimum value. No significant changes of this value are to be expected when an oxide richer in oxygen is formed.

6. Conclusions

A kinetic and fluodynamic description of processes that may take place near to the surface of some liquid metals in the presence of a gas flow containing definite amounts of oxygen has been given, with particular regard to the thermodynamic properties of the metal–oxygen system and the geometry of the experimental set-up commonly used in surface tension measurements. A complete theoretical treatment is presented in the Appendices 1 and 2 to this work. Low

TABLE 1 Selected values of $N^s_{O_2}$, θ_b and θ_m for the tin–oxygen system [4]

Temperature (K)	$N^s_{O_2}$ (mol cm^{-2} sec^{-1})			θ_b (h)			θ_m (h)		
	For $P^0_{O_2}$ MPa			For $P^0_{O_2}$ MPa			For $P^0_{O_2}$ MPa		
	$1.0\,10^{-21}$	$1.0\,10^{-11}$	$1.0\,10^{-7}$	$1.0\,10^{-21}$	$1.0\,10^{-11}$	$1.0\,10^{-7}$	$1.0\,10^{-21}$	$1.0\,10^{-11}$	$1.0\,10^{-7}$
1105	$9.7\,10^{-32}$	$8.8\,10^{-21}$	$5.1\,10^{-19}$	$3.2\,10^{22}$	$3.5\,10^{11}$	$6.2\,10^{9}$	$8.6\,10^{18}$	$9.5\,10^{7}$	$1.6\,10^{6}$
905	$1.4\,10^{-25}$	$1.4\,10^{-15}$	$1.4\,10^{-11}$	$1.5\,10^{15}$	$1.5\,10^{6}$	15.64	$5.9\,10^{12}$	592	$5.9\,10^{-2}$
705	$2.7\,10^{-25}$	$2.7\,10^{-15}$	$2.7\,10^{-11}$	$1.23\,10^{13}$	1238	0.12	$3.04\,10^{12}$	304	$3.04\,10^{-2}$
505	$6.7\,10^{-25}$	$6.7\,10^{-15}$	$6.7\,10^{-11}$	$2.8\,10^{9}$	1013	$2.81\,10^{-5}$	$1.24\,10^{12}$	124	$1.24\,10^{-2}$

flow rate conditions have been considered, being the ones usually imposed during most experiments.

Having selected one reaction in particular, on the basis of thermodynamic stability of all possible oxides which can form under the given boundary conditions, the kinetic features of the process can be described, in terms of the corresponding reaction regimes, according to the value of the parameters ϕ^2 and ε^0. Layouts are given in Figs 4 to 8.

From such diagrams the following information is immediately available:

1. The range of $P^0_{O_2}$ and T in which the reaction considered is thermodynamically possible.
2. The possible evolution in this field, from a kinetic point of view, as a function of $P^0_{O_2}$ and T.

In particular, once calculated the values of $\log \phi^2$ and $\log \varepsilon^0$ corresponding to a set of $P^0_{O_2}$, T values, it is possible to foresee all evolutions deriving from $P^0_{O_2}$ variations at the same temperature simply by graphic extrapolation or interpolation. Therefore, the treatment presented here, and applied to many cases of technological interest, allows one to define:

1. The physical and chemical equilibrium conditions of a system initially constituted by a liquid metal and oxygen, in the presence of an inert carrier, under total pressures ranging from about 10^{-4} to 0.1 MPa, for any flow rate.
2. The kinetic and fluodynamic characteristics of the process through which the equilibrium conditions are reached, having been given the geometry of the experimental set-up.

In order to obtain a complete generalization of the subject, an analogous theory should be developed for CO–CO_2 buffer mixtures, where the equilibrium exists.

$$CO + \tfrac{1}{2} O_2 = CO_2 \qquad (17)$$

In this case, feeding of oxygen to the reaction layer, no matter where it is placed, is no longer due exclusively to diffusion from a "reservoir". It can also proceed *in situ* from the displacement of equilibrium, Equation 17, according to Le Chatelier's principle.

Moreover, the vacuum as an operating condition is also left out of the aims of the present paper; which refers to pressure under which the mean free paths of particles are smaller than the thickness, δ_t, of the effective film. An extension of the present study to these two particular cases is presently under way [21].

Acknowledgement

This work was conducted with the support of the Progetto Finalizzato "Special Materials for Advanced Technologies" of the Italian National Research Council.

References

1. C. H. P. LUPIS "Chemical thermodynamics of materials", (Elsevier Amsterdam, Holland, 1983) p. 405.
2. E. T. TURKDOGAN, P. GRIEVESON and L. S. DARKEN, *J. Phys. Chem.* **67** (1963) 1647.
3. K. NOGI, K. OGINO, A. MCLEAN and W. A. MILLER, *Met. Trans. B* **17** (1986) 163.
4. A. PASSERONE, E. RICCI and R. SANGIORGI, *J. Mater. Sci.* **25** (1990) 4266.
5. P. COSTA, E. RICCI and A. PASSERONE, *High Temperatures–High Pressures* **20** (1988) 59.
6. J. F. PADDAY in "Surface and colloid science", Vol. 1, edited by E. Matijevic, (Wiley Interscience, New York, 1969) p. 101.
7. D. A. FRANK-KAMENETSKII, "Diffusion and heat exchange in chemical kinetics", (Princeton University Press, New Jersey, 1955) translated by N. Thon, p. 23.
8. E. E. PETERSEN, "Chemical reaction analysis", (Prentice Hall, Englewood Cliffs, New Jersey, 1965) p. 51.
9. O. LEVENSPIEL, "Chemical reactions engineering", (Wiley, New York, 1972) p. 477.
10. G. ASTARITA "Mass transfer with chemical reactions", (Elsevier, Amsterdam, Holland, 1967).
11. P. V. DANKWERTS, "Gas liquid reactions" (McGraw-Hill, New York, 1970).
12. Y. AUSTIN CHANG and KER-CHANG HSIEH, "Phase diagrams of ternary Copper–oxygen–metal systems", (ASM International, Metals Park, Ohio, 1989) p. 19.
13 T. B. MASSALSKI, J. L. MURRAY, L. H. BENNET and H. BAKER, "Binary alloy phase diagrams", (ASM International, Metals Park, Ohio, 1986) p. 1784.
14. O. KNACKE, O. KUBASCHEWSKI and K. HESSELMANN, "Thermo-chemical Properties of inorganic substances" 2nd Edn, (Springer Verlag, Dusseldorf, 1991).
15. D. W. G. WHITE, *Trans. Met. Soc. AIME* **236** (1966) 796.
16. V. I. NIZHENKO, L. I. SKLYARENKO and V. N. EREMENKO, *Ukr. Khim. Zh.* **6** (1965) 559.
17. S. C. HARDY, *J. Cryst. Growth* **71** (1985) 602.
18. L. GOUMIRI and J. C. JOUD, *Acta Met.* **30** (1982) 1397.
19. R. SANGIORGI, C. SENILLOU and J. C. JOUD *Surface Science* **202** (1988) 509.
20. S. OTSUKA and Z. KOZUKA, *Trans. Jpn. Inst. Met.* **22** (1981) 558.
21. P. CASTELLO, E. RICCI, A. PASSERONE and P. COSTA, *J. Mater. Sci.*, submitted.

Received 26 February 1993
and accepted 31 August 1993

Appendix 1 Evaluation of the concentration profile of the reactive gas along the chamber and of the effective film thickness

The most critical aspect of the application of the effective film theory to the model presented in this work is the correct evaluation of the thickness of the effective film and of the effective oxygen pressure at the external border of the diffusion layer. The problem can be satisfactorily faced by considering in some detail the transport phenomenon which oxygen undergoes in reaching the metal surface. At first no reaction will be taken into account, while explicit reference will be made to the geometry and the flow conditions of the system.

Let us consider a spherical drop of liquid metal having diameter, d_d, placed at the centre of a tube of diameter, d_t, and length, $2L$; a gas containing a reactive element A is introduced from one side of the tube, and flows along the tube, grazing the drop (Fig. 1). The concentration, of A in the supplying gas is C^0_A.

Assuming the abscissa of the centre of the drop is the origin of a co-ordinate system, the A flux at x is given by:

$$C_A(x)v_l - D_A \frac{dC_A(x)}{dx} = C^0_A v_l, \qquad -L \le x \le 0 \qquad (A1)$$

This flux is constant and contains the sum of two terms: a bulk flow term and a diffusive term. The gas flow is described in terms of the mean velocity, v_l, while a more detailed model should contain the velocity distribution in the tube section; such a complication, however, seems to be out of the scope of this paper.

Defining the concentration of reactive element A near the drop, as C_A^* and integrating we obtain:

$$C_A(x) = C_A^0 - (C_A^0 - C_A^*)\exp(v_l x/D_A) \quad \text{(A2)}$$

A rough estimation of C_A^* can be derived from the material balance around the drop:

$$v_l S_t C_A^0 = v_l S_t C_A^* + \frac{D_A}{\delta_{film}} S_d C_A^* \quad \text{(A3)}$$

Where S_t is the tube section, and δ_{film} is the thickness separating the interface from the first point at $P_{O_2}^*$.

Examining the concentration profile of A along a vertical axis, we expect to find an increase from a C_A^a value defined as the gas concentration liquid surface, up to a point in which the A concentration remains constant and equal to C_A^*.
tion remains constant and equal to C_A^*.

The length separating the surface from that point is assumed to be the δ_{film} parameter, which can be derived from the mass transfer coefficient for the system gas–drop:

$$\delta_{film} = \frac{d_d}{Sh} \quad \text{(A4)}$$

where Sh is the Sherwood number.

When $Re < 1$ we have simply $Sh = 2$ and $\delta_{film} = d_d/2$. Assuming $Pe_{film} = v_l \delta_{film}/D_A$ and defining a "shape factor" $f = S_t/S_d = d_t^2/d_d^2$, Equation A3 and, in turn A2 can be written as:

$$C_A^* = C_A^0 \frac{f Pe_{film}}{1 + f Pe_{film}} \quad \text{(A5)}$$

Substituting this relationship in Equation A2 an equation giving the concentration profile along the tube is obtained:

$$C_A(x) = C_A^0 \left\{1 - \frac{\exp[Pe_t(x/L)]}{1 + f Pe_{film}}\right\} \quad \text{for } -L \le x \le 0 \quad \text{(A6)}$$

At the entrance of the tube, that is for $x = -L$, the concentration of A is therefore:

$$C_A^e = C_A^0 \left[1 - \frac{\exp(-Pe_t)}{1 + f Pe_{film}}\right] \quad \text{(A7)}$$

where e is a quantity referred to the atmosphere at the entrance of the tube.

On the basis of these relationships, criteria allowing the most correct evaluation of the thickness, δ_t, of the diffusion layer, depending on the geometry of the experimental set-up and on the flow conditions can be established.

From Equation A6 we obtain:

$$-\left.\frac{dC_A}{dx}\right|_{x=0} = C_A^0 \frac{Pe_t}{L} \frac{1}{1 + f Pe_{film}} \quad \text{(A8)}$$

The A flux created *by diffusion only* at $x = 0$ ($C_A = C_A^*$) can be approximated in terms of an *effective diffusion layer*, Δx; so the following relationships can be written:

$$D_A C_A^0 \frac{Pe_t}{L} \frac{1}{1 + f Pe_{film}} = \frac{D_A}{\Delta x}(C_A^e - C_A^*) \quad \text{(A9)}$$

And, remembering (A7),

$$\Delta x = \frac{L}{Pe_t}[1 - \exp(-Pe_t)] \quad \text{(A10)}$$

A parameter δ_t can be then defined which expresses the effective length of the diffusive path:

$$\delta_t = \delta_{film} + \Delta x \quad \text{(A11)}$$

So that the following relationship can be derived between the parameters δ_t and δ_{film}:

$$\frac{\delta_t - \delta_{film}}{\delta_{film}} = \frac{1 - \exp(-Pe_t)}{Pe_{film}} \quad \text{(A12)}$$

Being necessarily $Pe_t > Pe_{film}$, three cases can be distinguished:

1. $1 \ll f Pe_{film} < Pe_t$. The right hand side of Equation A12 is negligible. Moreover, from Equations A5 to A7, $C_A^0 \approx C_A^e \approx C_A^*$ results; i.e. $C_A^p = C_A^0$; the diffusion layer is strictly confined around the drop, being $\delta_t \cong \delta_{film}$, and, under creeping flow conditions, $\delta_t \approx d_d/2$. Transport along the tube is linked basically to dynamic flow.

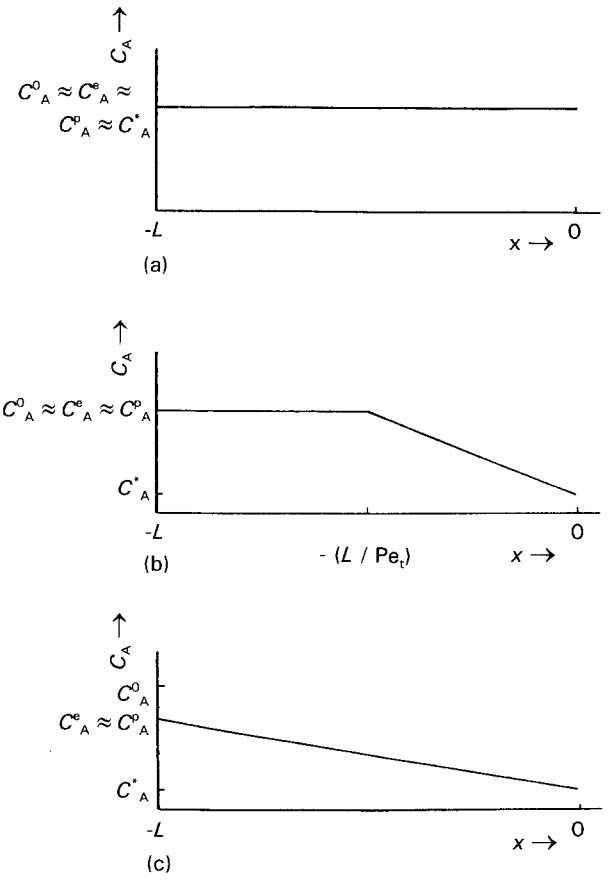

Figure 11 Possible diffusion profiles along the measurement chamber. (a) condition 1, $1 \ll f Pe_{film} \ll Pe_t$; (b) condition 2, $f Pe_{film} \ll 1 \ll Pe_t$; (c) condition 3, $f Pe_{film} < Pe_t \ll 1$.

2. $f\mathrm{Pe}_{\mathrm{film}} \ll 1 \ll \mathrm{Pe}_t$. From Equations A5 and A7 one has $C_A^* \ll C_A^0$; $C_A^e \approx C_A^0$. A value for C_A^p can be assumed between C_A^0 and C_A^*; for instance, at $C_A^p \cong 0.5C_A^0$, then (see Equations A5 and A6) the diffusive flow and the bulk flow are equal.

Now the term on the right in Equation A12 is no longer negligible; i.e. transport along the tube is due to diffusion, more than to flow, up to a distance $\delta_t = L/\mathrm{Pe}_t = D_A/v_l$ from the drop.

3. $f\mathrm{Pe}_{\mathrm{film}} < \mathrm{Pe}_t \ll 1$. Now the term on the right in Equation A12 is large, and diffusion is the main transport mechanism along the whole tube, so that $\delta_t = L$. Both C_A^e and C_A^* are much less than C_A^0 and one can put $C_A^p = C_A^e \approx C_A^0(Pe_t + f\mathrm{Pe}_{\mathrm{film}})$. A schematic layout of the concentration profiles for conditions 1 to 3 is given in Fig. 11.

Appendix 2 Evaluation of reactive gas fluxes towards the liquid metal surface

In order to estimate the reactive gas flux at the liquid–vapour interface, N_A^s, the analogous quantity at the extreme border of the diffusion layer, N_A^p, has to be known.

Under reaction regimes A and B no enhancement of the reactive gas flux towards the liquid surface is to be expected. N_A^p being a flux calculated across the tube section and N_A^s a flux calculated across the drop surface, a factor, f, should be introduced in order to account for the ratio S_t/S_d. Thus, for regimes A and B, we have:

$$N_A^s \cong fN_A^p \tag{A13}$$

On the other hand, by applying the same reasoning used in Reference [5], for regimes C and D:

$$N_A^s = f(N_A^p + \alpha N_{\mathrm{met}}^p)\left[1 + \frac{D_{\mathrm{met}}P_{\mathrm{met}}^s\alpha^2}{D_A P_A^s \tau^{\alpha+1}}\right]^{-1} \tag{A14}$$

Where τ is 1 for $P_A^\sigma = P_A^s$, and $(\alpha + 1)^{1/\alpha}$ for $P_A^\sigma = 0$; P_A^σ being the actual value at the gas–liquid interface.

As a first approximation, the quantity N_{met}^p can be assumed to be equal to zero. Moreover, the quantity N_A^p is given, in general, by the following formula, deriving from Fick's law and modified by the addition of an "enhancement factor" Θ whose presence is due to the reaction, and whose value depends on the reaction regime:

$$N_A^p = \frac{P_A^p D_A \Theta}{RT\delta_t} \tag{A15}$$

where $\Theta = 1$ for regimes A and B; $\Theta = \phi$ for regime C; and $\Theta = 1 + \varepsilon$ for regime D.

Choosing the appropriate value of Θ and substituting the quantity N_A^p in Equation A13 (or Equation A14, according to the reaction regime considered), with the corresponding formula derived from Equation A15, the following general equations, giving the reactive gas flux at the liquid–gas interface, can be found:

Regimes A and B

$$N_A^s = f\frac{P_A^p D_A}{RT\delta_t} \tag{A16}$$

From the point of view of the reactive gas flux calculation, the case in which there are no reactions at all (i.e. for $P_{O_2}^0 < P_{O_2}^s$) is not different from the one of regime A. Thus, this formula can also be used for determining the reactive gas flux in those circumstances.

Regime C

$$N_A^s = f\frac{P_A^p D_A}{RT\delta_t}\phi\left(1 + \frac{D_{\mathrm{met}}P_{\mathrm{met}}^s\alpha^2}{D_A P_A^s \tau^{\alpha+1}}\right)^{-1} \tag{A17}$$

Regime D

$$N_A^s = f\frac{P_A^p D_A}{RT\delta_t}[1 + \varepsilon^0(P_A^0/P_A^p)]\left(1 + \frac{D_{\mathrm{met}}P_{\mathrm{met}}^s\alpha^2}{D_A P_A^s \tau^{\alpha+1}}\right)^{-1} \tag{A18}$$

Depending on the geometry of the experimental set-up, and on the flow parameters, the most correct expression of P_A^p in function of the experimentally accessible quantities P_A^0, $f\mathrm{Pe}_{\mathrm{film}}$, Pe_t can be derived from the equations presented in Appendix 1. Substituting it in Equations A16 to A18, formulae for calculation of the oxygen flux at the liquid–gas interface can be obtained that are the most adequate for any actual experimental set-up.

Appendix 3 Conditions of inaccessibility of reactive gas to the liquid metal surface: an example in the tin–oxygen system

Even when a condition of reactive gas accessibility to the liquid metal surface (regimes A and B) exists, the flux could be so low that no reliable effects on surface tension are observed during measurement. Presented here is an order of magnitude analysis of this effect for the tin–oxygen system.

Assuming that such an experiment lasts for about half-an-hour, and supposing that significant effects of oxygen adsorption could be observed when at least one-tenth of the surface sites have been occupied, it is possible to determine the minimum value of $P_{O_2}^0$ necessary to produce a significant lowering of surface tension. The condition required is:

$$\frac{\theta_m}{10} \leq 0.5\,\mathrm{h} = 1800\,\mathrm{s} \tag{A19}$$

Remembering Equation 15, this condition becomes:

$$\frac{0.1\Omega}{N_{O_2}^s} = \frac{3\,10^{-10}}{N_{O_2}^s} \leq 1800\,\mathrm{s} \tag{A20}$$

It follows that the limiting value of the oxygen flux required to produce a significant lowering of surface tension is:

$$N_{O_2}^s \geq 1.67\,10^{-13} \tag{A21}$$

Substituting $N_{O_2}^s$ with the general expression for a reactive gas in conditions of regimes A and B (Equation A16) and inserting the expression for $P_{O_2}^p$ obtained from Equation A6 when the condition $f\mathrm{Pe}_{\mathrm{film}} < \mathrm{Pe}_t \ll 1$ is verified (i.e. for low flow rates, e.g. in the case of Reference [4]), the following implicit

condition on $P^0_{O_2}$ is obtained:

$$N^s_{O_2} = \frac{P^0_{O_2}(Pe_t + f\,Pe_{film})D_A}{RT\delta_t} f \geq 1.67\,10^{-13} \quad (A22)$$

Under experimental conditions [4]: $v_l = 0.022$ cm s^{-1}, $\delta_t = 25$ cm, $\delta_{film} = 0.5$ cm and $f = 5$. Equation A22 becomes:

$$N^s_A = 1.5\,10^{-3}\frac{P^0_{O_2}}{T} \geq 1.67\,10^{-13} \quad (A23)$$

The limiting condition of surface accessibility is thus reached for:

$$P^0_{O_2} \geq 1.1\,10^{-10}T, \quad (A24)$$

Substituting this relationship in the definition for the parameter ε^0, the limiting condition itself can be written, at each temperature, in terms of the parameters ϕ^2 and ε^0, and consequently represented graphically on the kinetic–fluodynamic diagram (dashed line in Fig. 10).

For each value of $\phi^2(T)$ in the AB region, no significant effects of oxygen adsorption on the surface are expected for $\varepsilon^0 \leq (\alpha P^s_{met} D_{met}/1.1\,10^{-10} D_A(T)T)$.